SUPPLEMENTARY INFORMATION

Accessible detection of SARS-CoV-2 through molecular nanostructures and automated microfluidics

Haitao Zhao[1,#], Yan Zhang[1,2,#], Yuan Chen[1,2], Nicholas R.Y. Ho[1,3], Noah R. Sundah[1,2], Auginia Natalia[1,2], Yu Liu[1,2], Qing Hao Miow[4], Yu Wang[4], Paul A. Tambyah[4,5], Catherine W.M. Ong[1,4,5], Huilin Shao[1,2,3,6,*]

[1] Institute for Health Innovation & Technology, National University of Singapore, Singapore
[2] Department of Biomedical Engineering, Faculty of Engineering, National University of Singapore, Singapore
[3] Institute of Molecular and Cell Biology, Agency for Science, Technology and Research, Singapore
[4] Infectious Diseases Translational Research Programme, Department of Medicine, Yong Loo Lin School of Medicine, National University of Singapore, Singapore
[5] Division of Infectious Diseases, Department of Medicine, National University Hospital, Singapore
[6] Department of Surgery, Yong Loo Lin School of Medicine, National University of Singapore, Singapore
[#] These authors contributed equally

* Corresponding author
Huilin Shao, PhD
National University of Singapore
MD6, 14 Medical Drive
#14-01, Singapore 117599
(65) 6601 5885
huilin.shao@nus.edu.sg

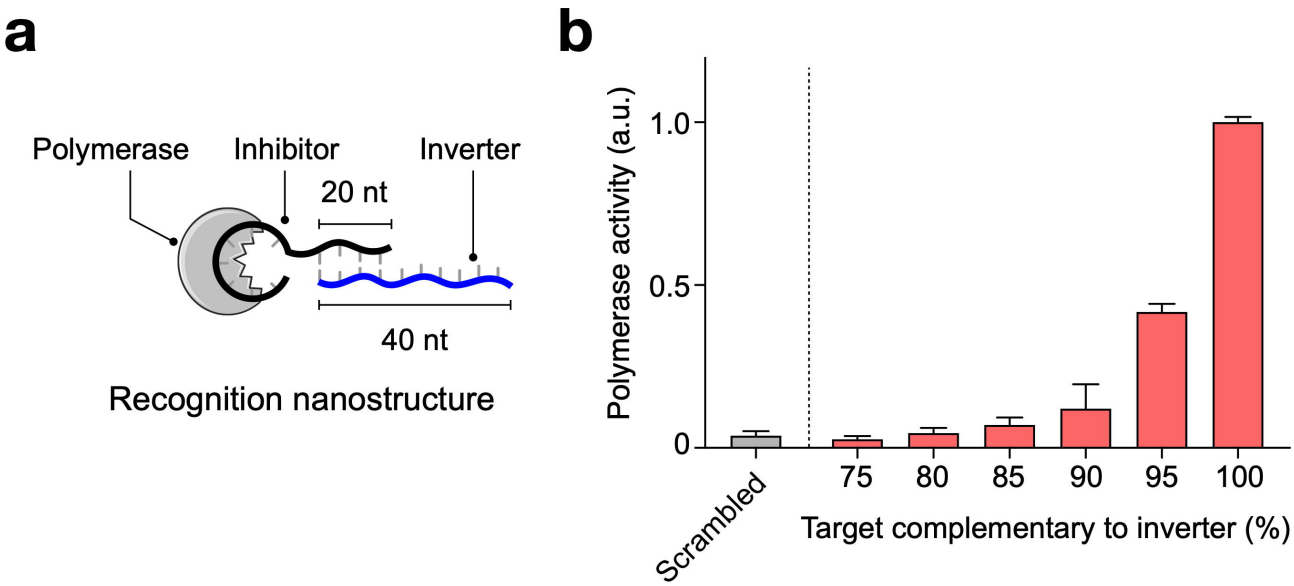

Supplementary Figure 1: Recognition nanostructure evaluation.
(a) Schematic of the recognition nanostructure. It comprises a Taq DNA polymerase bound with an inhibitor strand and an inverter strand. **(b)** Specificity of the nanostructure. Scrambled sequences as well as sequences bearing different degree of complementarity to the inverter were incubated with the recognition nanostructure. Fully complementary targets (100% = 40/40) resulted in strong polymerase activation. Less complementary targets (<95% or <38/40) resulted in significant reduction in polymerase activation.

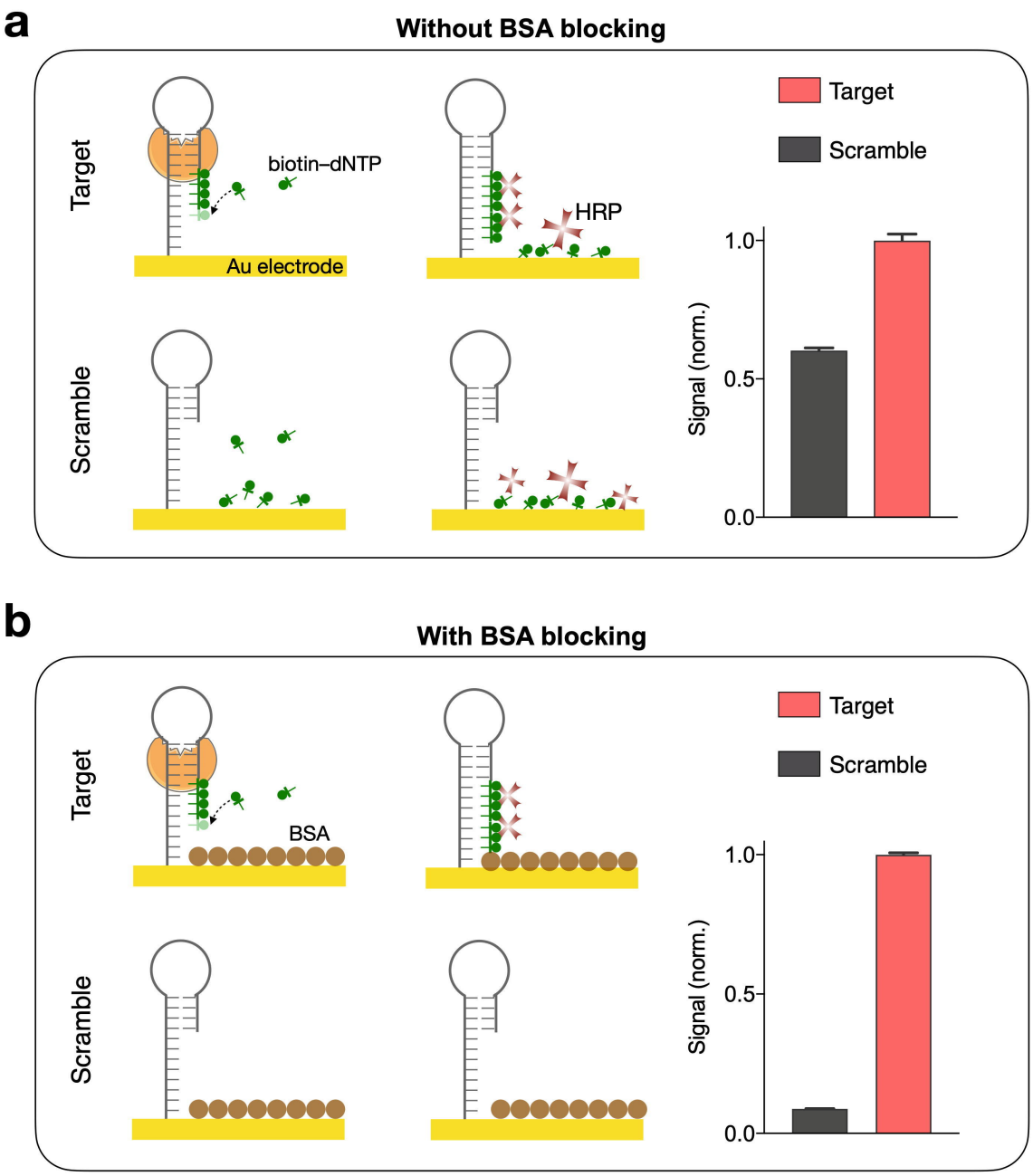

Supplementary Figure 2: Signal nanostructure evaluation.
(a) Without BSA blocking, HRP could nonspecifically bind to the electrode surface, even in the absence of complementary RNA target. **(b)** With BSA blocking, the non-specific binding is suppressed and thus the signal-to-noise ratio is improved.

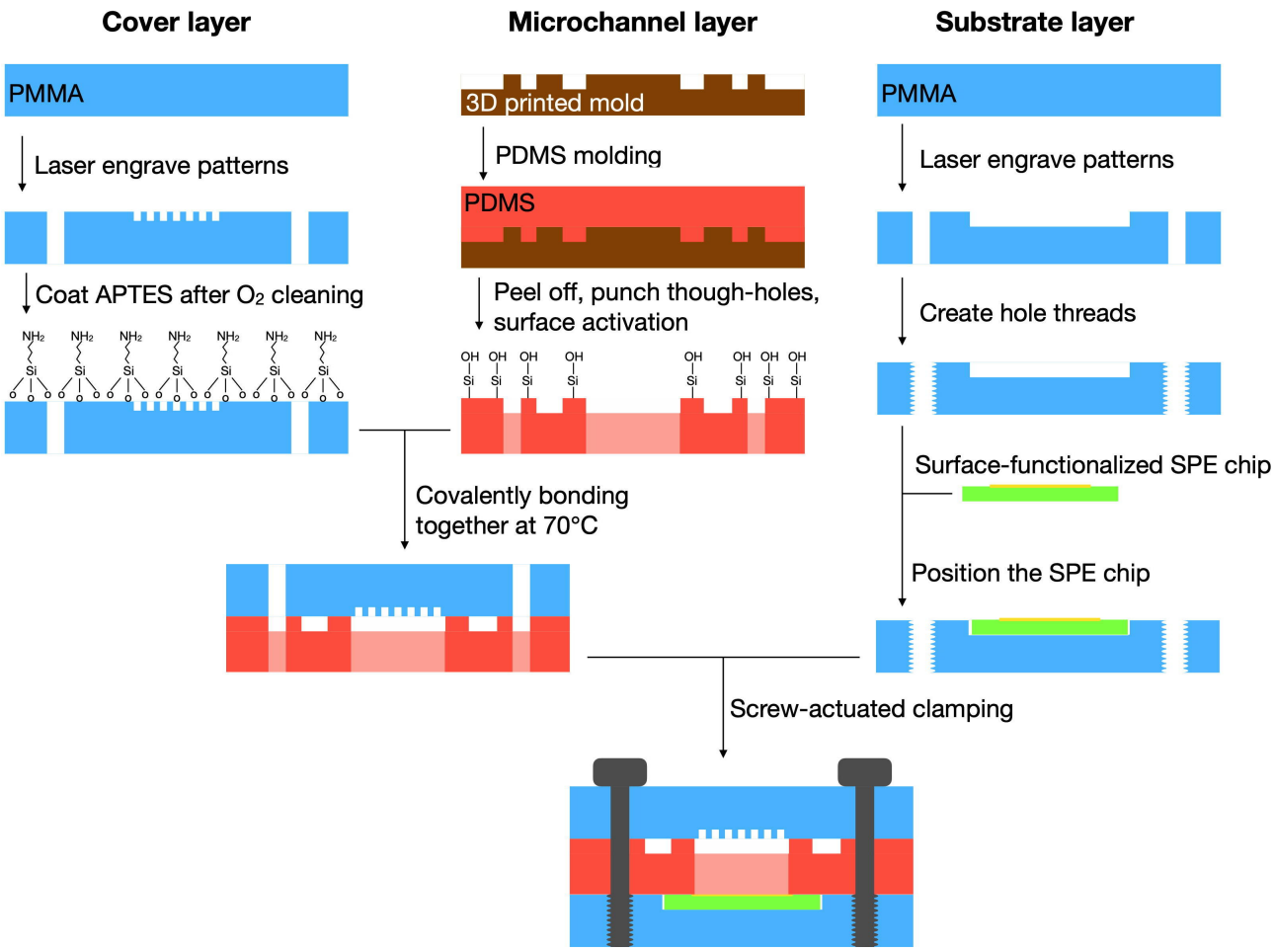

Supplementary Figure 3: eSIREN microfluidic chip fabrication.
The cover and substrate layers were made from PMMA sheets and constructed using a tabletop CO_2 laser engraver. The microchannel layer was fabricated through PDMS molding from a 3D-printed cast mold. To bond the cover and microchannel layers, the cover layer was coated with APTES after O_2 plasma cleaning, before attaching to the surface-activated microchannel layer overnight at 70°C. The three layers, along with the SPE chip, were bonded together through screw-actuated clamping.

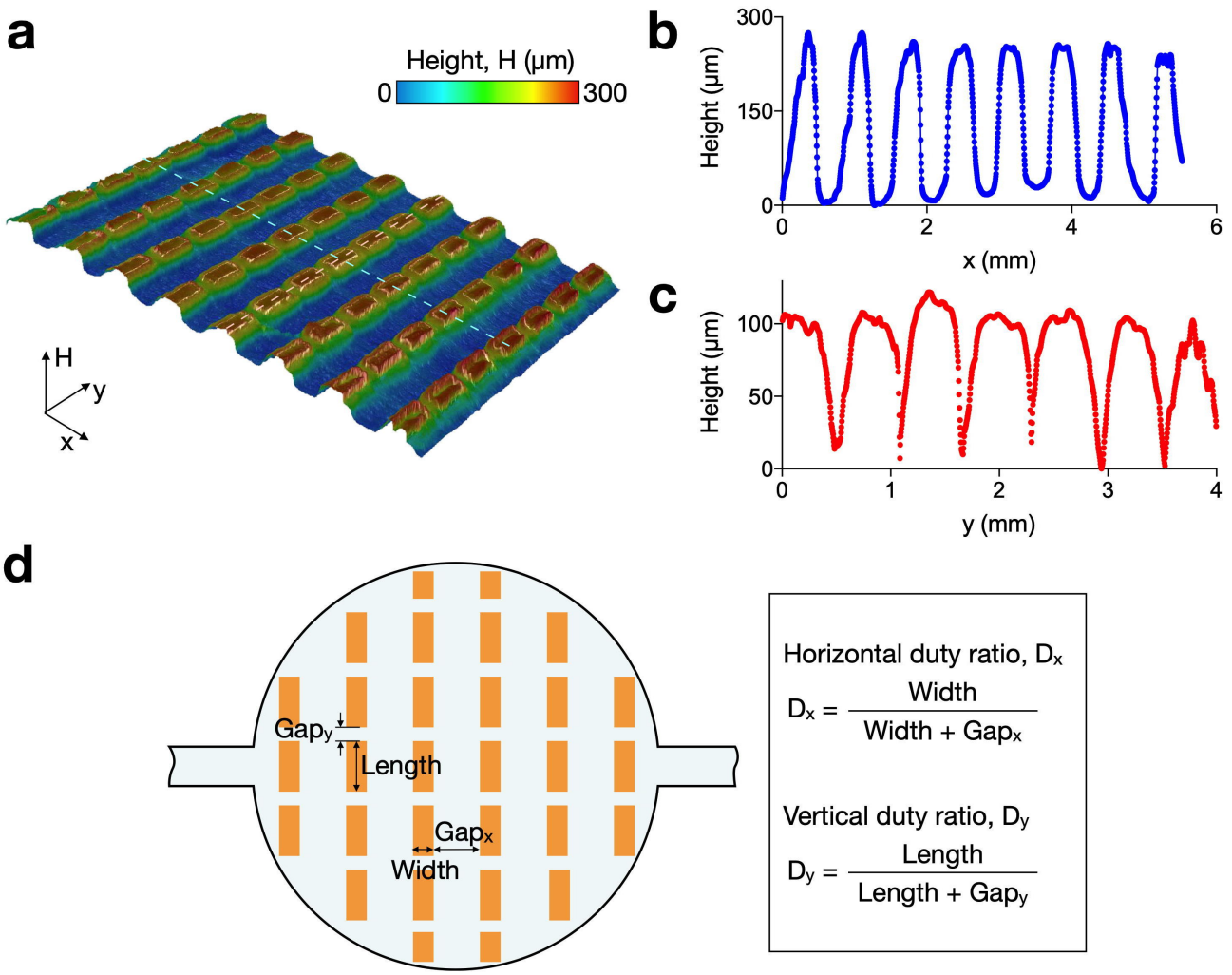

Supplementary Figure 4: Characterization of the liquid front guider.
(a) Surface profile of the guider measured with a digital microscope (Keyence VHX-6000). Height profiles in the **(b)** *x*-direction and **(c)** *y*-direction. **(d)** Definition of the horizontal and vertical duty ratios in charactering a liquid front guider.

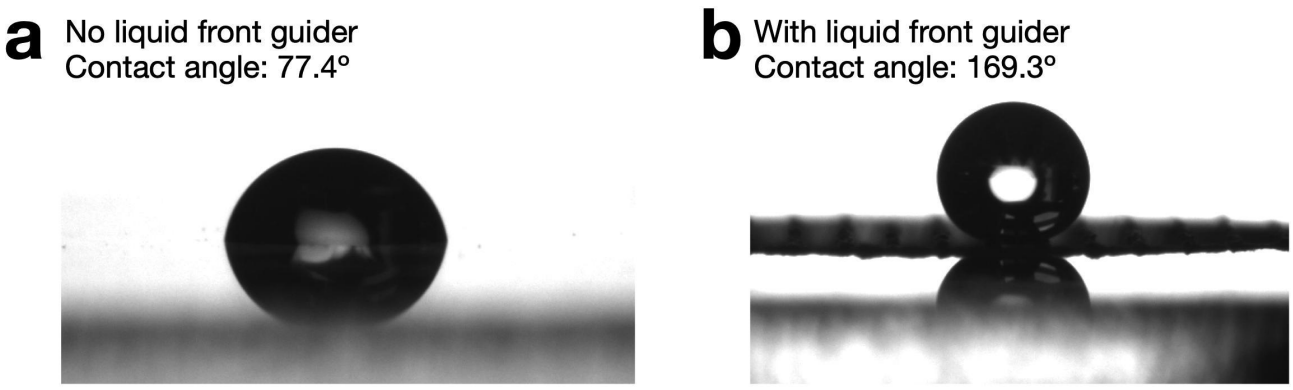

Supplementary Figure 5: Contact angle measurement.
Photographs of droplets on **(a)** a bare PMMA surface (without the liquid front guider) and **(b)** a PMMA surface with the liquid front guider.

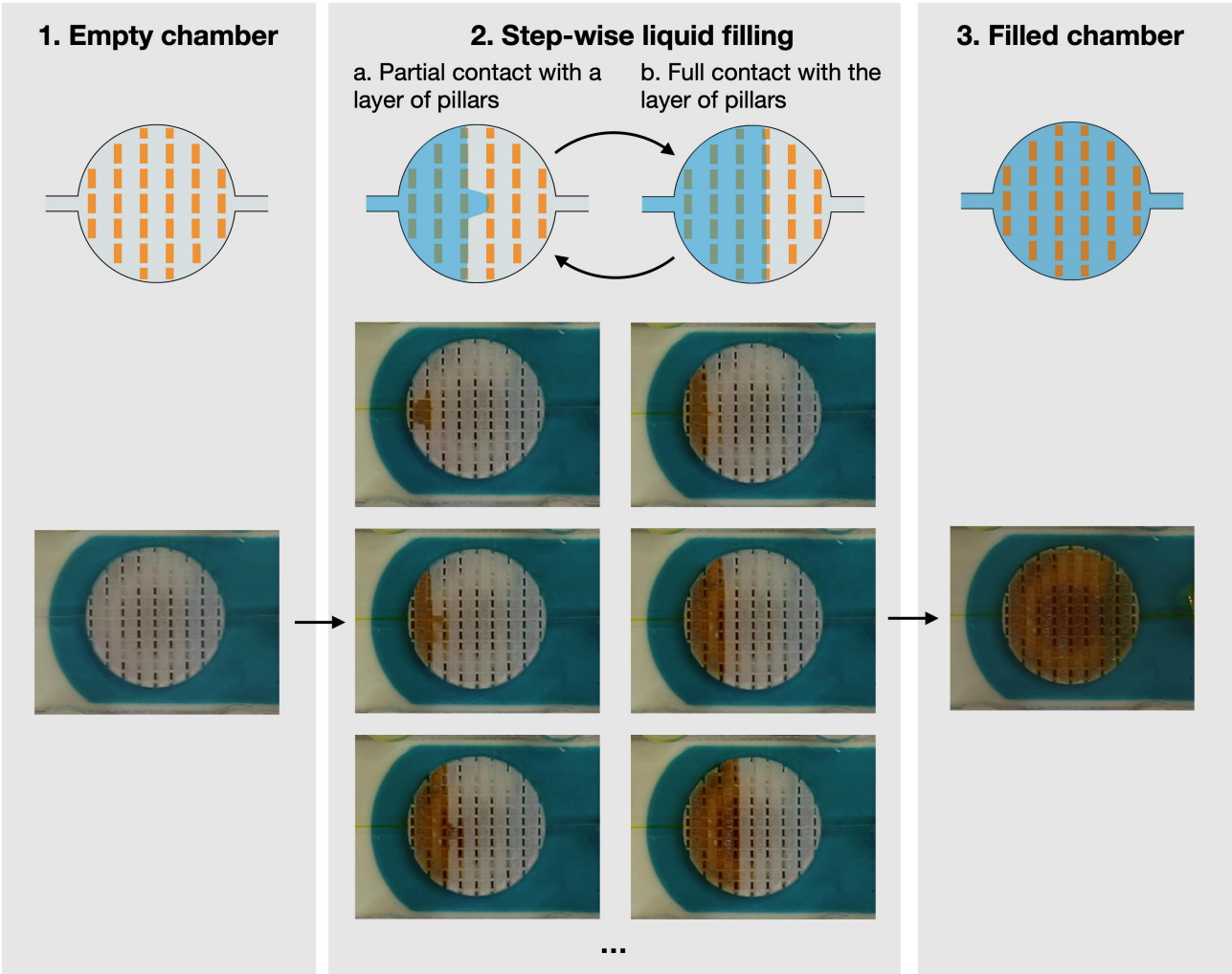

Supplementary Figure 6: Step-wise liquid filling in the reaction chamber.
When a liquid starts to contact a column of pillars, it experiences a resistive capillary force. The liquid is thus guided to move between the pillar layers, due to a smaller resistance, towards the chamber sidewall. Once the void between two pillar layers is completed filled, the liquid breaks the capillary resistance to fill the next interlayer space. With this step-wise filling process, large reaction chambers can be fully filled without bubble trapping.

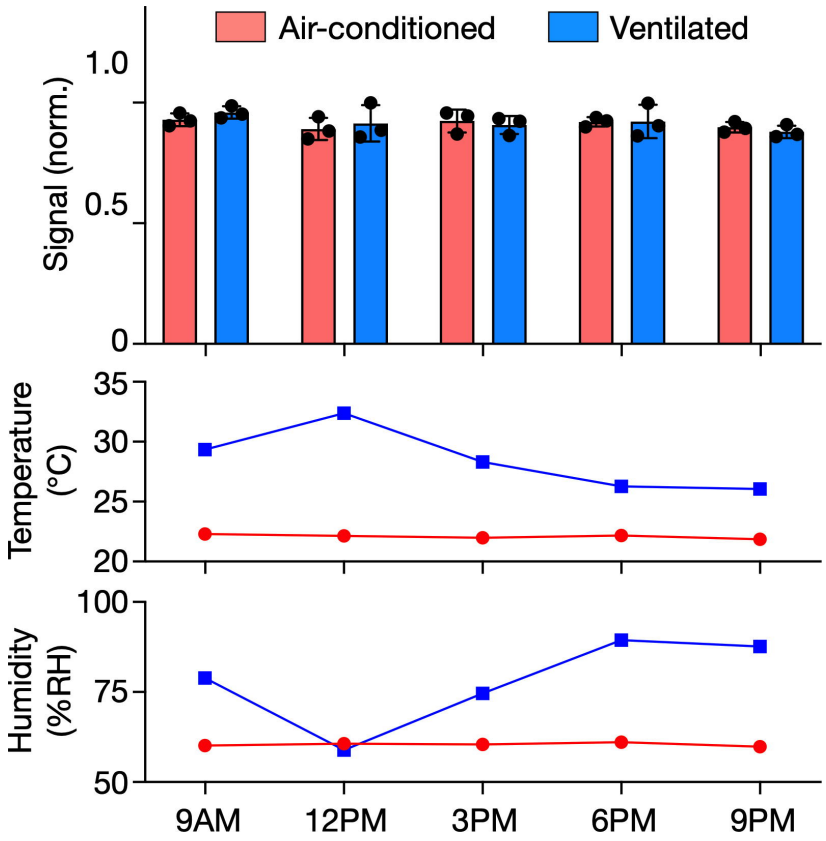

Supplementary Figure 7: Stability of the eSIREN platform.
eSIREN measurements were conducted with synthetic viral target at different times of a day, in air-conditioned and ventilated rooms. The eSIREN measurements show consistent readings despite temperature and humidity fluctuations.

Supplementary Table 1. Sequences of DNA nanostructures.

Description	Sequence
Signaling nanostructure	/5ThioMC6-D/GACAGTCGATCAGTACAATGCTACGCAT TGTCGATAGCTCTGTCGCTATCGACAATGCGT
Recognition nanostructure (Inhibitor sequence)	TTATTTGACTCCTGGTGATTCAATGTACAGTATTG
Recognition nanostructure (Inverter sequence)	AATCACCAGGAGTCAAATAACTTCTATGTAAAGCAAGTAA
Viral RNA target (SARS-CoV-2 *S* gene)	UUACUUGCUUUACAUAGAAGUUAUUUGACUCCUGGUGAUU
2 mismatch SARS-CoV-2 *S* gene synthetic target	UUACUUGCUUUACAUAGAAGUUAUUUGACU**AG**UGGUGAUU
4 mismatch SARS-CoV-2 *S* gene synthetic target	UUACUUGCUUUACAUAGAAGUUAUU**CUA**CU**A**GUGGUGAUU
6 mismatch SARS-CoV-2 *S* gene synthetic target	UUACUUGCUUUACAUAGAAGUUAUU**CU**ACU**AG**UGGU**CU**UU
8 mismatch SARS-CoV-2 *S* gene synthetic target	UUACUUGCUUUACAUAGAAGUUAUU**CU**ACU**AG**U**AC**U**CU**UU
10 mismatch SARS-CoV-2 *S* gene synthetic target	UUACUUGCUUUACAUAGAAGUUAUU**CU**A**UGAG**U**AC**U**CU**UU
Scramble	GUCAUGUGCUCACGGAACUUACUGUAUGAGUAGUGAUUUG

Supplementary Table 2. Comparison of eSIREN and colorimetric detection.

	eSIREN	Colorimetric defection*
Signal format	Electrochemical	Visual color
Limit of detection (nucleic acid copies)	7 copies/μl	4×10^5 copies/μl
Clinical accuracy (AUC)	0.962 for SARS-CoV-2	0.965 for HPV16 0.944 for HPV18
Implementation	- Miniaturized pumping system to automate assay operation - Delicate mechanisms (vacuum loader, liquid front guider, pressure actuation, etc.) for improved robustness	- Manual assay operation - No mechanism to improve system robustness
Application	- Point-of-care diagnostics - Disease with trace amounts of pathogen nucleic acids (e.g., SARS-CoV-2)	- Point-of-care diagnostics - Disease with moderate amounts of pathogen nucleic acids (e.g., HPV, HBV)

* Ho, N. R. Y. et al. Visual and modular detection of pathogen nucleic acids with enzyme-DNA molecular complexes. *Nat. Commun.* **9**, 3238 (2018).